

**ac electric fields drive steady flows in flames**Aaron M. Drews,<sup>1</sup> Ludovico Cademartiri,<sup>2</sup> Michael L. Chemama,<sup>3</sup> Michael P. Brenner,<sup>3,4</sup>  
George M. Whitesides,<sup>2,4</sup> and Kyle J. M. Bishop<sup>1,\*</sup><sup>1</sup>*Department of Chemical Engineering, Pennsylvania State University, University Park, Pennsylvania 16802, USA*<sup>2</sup>*Department of Chemistry and Chemical Biology, Harvard University, Cambridge, Massachusetts 02138, USA*<sup>3</sup>*Harvard School of Engineering and Applied Sciences, Cambridge, Massachusetts 02138, USA*<sup>4</sup>*Kavli Institute, Harvard University, Cambridge, Massachusetts 02138, USA*

(Received 6 June 2012; published 20 September 2012)

We show that time-oscillating electric fields applied to plasmas present in flames create steady flows of gas. Ions generated within the flame move in the field and migrate a distance  $\delta$  before recombining; the net flow of ions away from the flame creates a time-averaged force that drives the steady flows observed experimentally. A quantitative model describes the response of the flame and reveals how  $\delta$  decreases as the frequency of the applied field increases. Interestingly, above a critical frequency, ac fields can be used to manipulate flames at a distance without the need for proximal electrodes.

DOI: [10.1103/PhysRevE.86.036314](https://doi.org/10.1103/PhysRevE.86.036314)

PACS number(s): 47.70.-n, 52.30.-q, 47.70.Pq

**I. INTRODUCTION**

The most familiar description of a flame is “a local region of high temperature generated by rapid, exothermic chemical reactions.” A flame is, however, also a plasma. In particular, the combustion of hydrocarbon fuels generates sufficient densities of charged species that even small flames (the flame of a humble candle) can be considered as chemically driven, nonequilibrium plasma [1]. As such, flames interact with external electric fields, which can be used to monitor [2], manipulate [3,4], and enhance [5,6] the processes that make up combustion through a variety of physical and chemical mechanisms. Sufficiently strong electric fields (greater than  $\sim 10^6$  V/m at atmospheric pressure) influence the chemistry of combustion by accelerating electrons to energies capable of exciting, dissociating, or ionizing neutral species upon impact [6]. Even fields that are too weak to influence combustion directly can cause significant hydrodynamic flows [1]—so-called electric or ionic winds [7]—through the collisional transfer of momentum from accelerated charged species to the neutral gas [8,9].

Previous efforts to manipulate flames with electric winds have relied almost exclusively on static (dc) fields [1] to induce steady currents of charged species that drive steady gas flows (although see Refs. [4,10,11]). Despite promising demonstrations (e.g., enhancing flame stability [5], manipulating heat transfer [3], and reducing pollutant emissions [12]), the magnitude of these effects, as well as their applicability, is strictly limited by ionic screening, which requires direct contact of the electrodes and the flame to maximize the ionic currents and gas velocities [8].

Here we report that time-oscillatory (ac) electric fields also induce steady electric winds in flame plasmas with gas velocities exceeding those due to static fields of comparable magnitude. Furthermore, unlike static fields, the electric force due to ac fields is localized near the surface of the flame. Consequently, the ac response depends only on the field at the location of the flame, not on the position of the electrodes

used to generate the field. These results suggest that ac fields can be used to manipulate and control combustion processes at a distance.

To characterize and explain this effect, we investigated a simple experimental system comprising a laminar methane-air flame positioned between two parallel-plate electrodes. We quantify both the electric and hydrodynamic response of the flame as a function of frequency and magnitude of the applied field. A theoretical model shows how steady gas flows emerge from the time-averaged electrical force due to the field-induced motion of ions generated within the flame and by their disappearance by recombination. Our predictions of both the flow velocity and the electric response agree quantitatively with the experimental results.

**II. EXPERIMENT**

A small methane flame was positioned symmetrically between two parallel aluminum electrodes ( $20 \times 20$  cm<sup>2</sup>), separated by a distance  $L = 10$  cm (Fig. 1). The burner was a thermally and electrically insulating cylindrical tube (alumina composite with 6.4 mm i.d. and 9.5 mm o.d.) through which flowed a mixture of methane, oxygen, and nitrogen [molar composition, CH<sub>4</sub>:O<sub>2</sub>:N<sub>2</sub> = 0.15:0.17:0.68 with a flow rate of 500 SCCM (where SCCM denotes cubic centimeter per minute at STP) and equivalence ratio,  $\phi = 1.75$ , with air as oxidizer]. When needed, the nitrogen stream was doped with a fine mist (1–10  $\mu$ m droplets, created by an ultrasonicator) of 1M aqueous NaOH to increase the density of ions within the flame [13,14]. To mitigate external air flows, we enclosed the flame and the electrodes in a glass box ( $30 \times 30 \times 30$  cm<sup>3</sup>) with a central, triangular opening ( $\sim 20$  cm) in its top to vent combustion products.

A high-voltage amplifier (Trek 40/15) applied sinusoidal, time-varying electric fields to the flame. ac fields caused the transient redistribution of charged species generated within the flame and resulted in the formation of two gas jets directed symmetrically outward toward the two electrodes [Fig. 1(b)]. To characterize the response of the flame, we measured two quantities: (i) the electric current  $I$  through the circuit

\*kjmbishop@enr.psu.edu

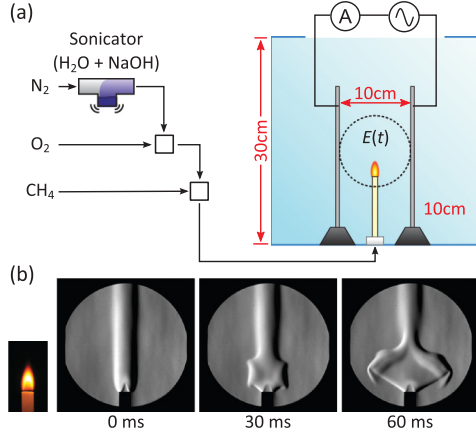


FIG. 1. (Color online) (a) Schematic illustration of the experimental setup; the cubic combustion chamber is drawn to scale. The dotted circle illustrates the field of view for the schlieren images below. (b) Schlieren images of a premixed, NaOH-doped methane flame following the application of an oscillating electric field of magnitude  $100 \text{ kV}_{\text{rms}}/\text{m}$  at 1 kHz.

illustrated in Fig. 1(a) and (ii) the velocity of the field-induced gas flows using high-speed schlieren velocimetry [15,16].

### III. STATIC FIELDS

As previously reported [1,8], the application of a static field to a methane flame creates an electric wind (Fig. 2). Positive and negative charge carriers generated within the flame (mostly  $\text{CHO}^+$ ,  $\text{H}_3\text{O}^+$ ,  $\text{C}_2\text{H}_3\text{O}^+$ , and  $\text{CH}_5\text{O}^+$  ions [17]; electrons, and  $\text{O}_2^-$ ,  $\text{OH}^-$ ,  $\text{O}^-$ ,  $\text{CHO}_2^-$ ,  $\text{CHO}_3^-$ , and  $\text{CO}_3^-$  ions [18]) drift toward the respective electrodes. The accumulation of charge on both sides of the flame results in an electric force density  $f = \rho E$  ( $\rho$  is the charge density and  $E$  is the local electric field) that drives two jets of gas in opposite directions. To contrast this dc response with the ac effect described below, we briefly quantify the effect of static electric fields.

The electric force density  $f$  driving the flow is directly proportional to the electric current  $I$ , which can be measured directly [Fig. 2(b)]. This proportionality holds within regions of space charge on both sides of the flame where charge carriers of one polarity greatly outnumber those of opposite polarity. The electric force and the current density can therefore be approximated as  $f \approx q_{\pm} n_{\pm} E$  and  $j \approx q_{\pm} K_{\pm} n_{\pm} E \sim I$ , where  $q_{\pm}$ ,  $n_{\pm}$ , and  $K_{\pm}$  are the charge, number density, and mobility (drift velocity divided by field strength) of the charge carriers.

For the methane flame without NaOH dopant, the current increases quadratically with the field before saturating at a constant value. At low fields, the redistribution of charged species acts to screen the field in the region of the flame and limits the current. Within the space-charge regions, the ion density is proportional to the applied field  $n_{\pm} \sim E_0$  and the current scales as  $j \sim E_0^2$  [1,8,16]. For sufficiently strong fields, the current is instead limited by the rate of ionization within the flame; that is, all charged species generated by combustion are removed by the field via the electrodes. By doping the flame with additional ions, the transition from the space-charge-limited regime to the reaction-limited regime can be shifted to larger fields [Fig. 2(b)].

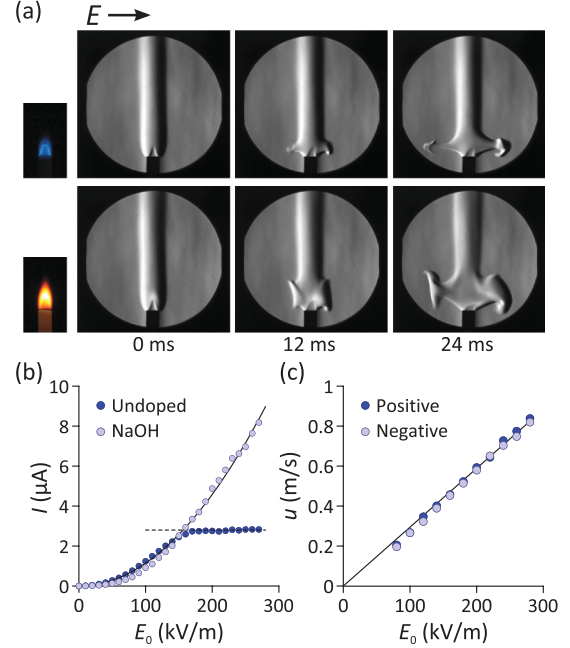


FIG. 2. (Color online) Static fields. (a) Schlieren images of a premixed methane flame without (top) and with (bottom) NaOH dopant directly after the application of a static electric field of  $280 \text{ kV}/\text{m}$ . (b) Electric current as a function of the applied field strength for a premixed methane flame with and without ion doping. The solid and dashed lines illustrate the space-charge-limited and reaction-limited responses, respectively; the fit used for the space-charge response is  $I = (1.1 \times 10^{-16} \text{ A m}^2 \text{ V}^{-2}) E_0^2$ . (c) Characteristic gas velocity  $u$  as a function of field strength for the NaOH-doped flame; “positive” and “negative” refer to the sign of the charged species driving the jet. The solid curve is  $u = (2.9 \times 10^{-6} \text{ m}^2 \text{ V}^{-1} \text{ s}^{-1}) E_0$ .

In the space-charge-limited regime, the velocities of the gas jets increase linearly with the magnitude of the applied field [Fig. 2(c)] as explained by Bernoulli’s principle [1]. Briefly, the pressure drop is proportional to the electric force  $\Delta p \sim f$ , which in turn is proportional to the current density  $f \sim j$ , such that  $\Delta p \sim j \sim E_0^2$ . The characteristic velocity is therefore  $u = (\Delta p / 2\rho_f)^{1/2} = C E_0$ , where  $\rho_f$  is the fluid density and  $C$  is a constant. Assuming  $\Delta p \approx \epsilon_0 E_0^2$  (see below), these scaling arguments suggests  $C \approx 3.9 \times 10^{-6} \text{ m}^2 \text{ V}^{-1} \text{ s}^{-1}$ , in agreement with experiment [Fig. 2(c)].

### IV. OSCILLATING FIELDS

Application of an ac field  $E(t) = \sqrt{2} E_0 \cos(\omega t)$  to a doped flame creates two gas jets similar to those produced by a static field [Fig. 1(b)]. Because the applied field is symmetric, the jets are nearly identical in shape and their velocity increases strongly with increasing field strength  $E_0$  and weakly with increasing frequency  $\nu$  [Fig. 3(a)]. At low frequencies, the gas velocity is well described by the dc relation from Fig. 2(c). At higher frequencies, the velocity increases by approximately 20% at the highest frequencies accessible by the amplifier ( $\sim 1 \text{ kHz}$ ).

To characterize the electric response of the flame, we calculated the energy dissipation rate  $\Phi = \langle I(t)V(t) \rangle$  due to the motion of charged species in and around the flame as a

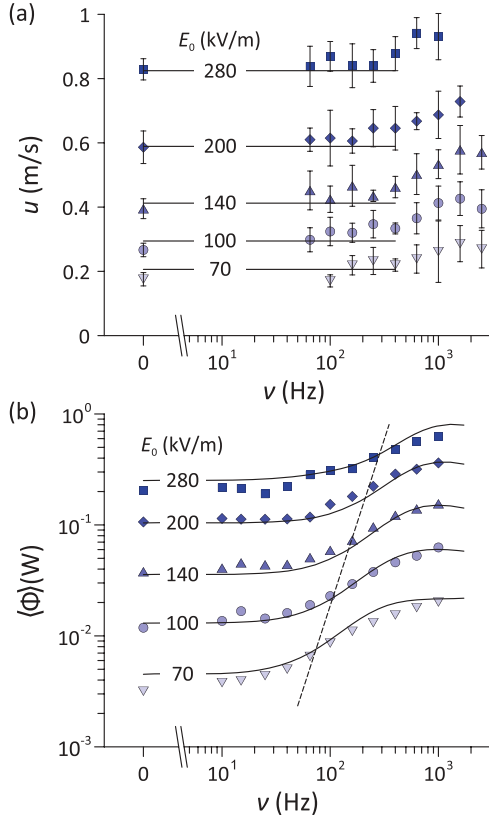


FIG. 3. (Color online) Oscillating fields applied to NaOH-doped, premixed methane flames. (a) Characteristic gas velocity  $u$  as a function of frequency  $\nu$  and field strength  $E_0$ . The solid lines correspond to  $u = (2.9 \times 10^{-6} \text{ m}^2 \text{ V}^{-1} \text{ s}^{-1})E_0$  as obtained from Fig. 2(c). (b) Average electric dissipation rate  $\Phi$  as a function of frequency  $\nu$  and field strength  $E_0$ . The solid lines are theoretical predictions of the charge transport model. The dashed line illustrates the transition from the low-frequency regime to the high-frequency regime as defined by the condition  $\delta \sim L$ . The parameters used in the model are as follows: electrode spacing,  $L = 0.1$  m; flame width,  $b = 10^{-2}$  m; flame thickness,  $a = 10^{-4}$  m; mobility,  $K = 1.05 \times 10^{-4} \text{ m}^2 \text{ V}^{-1} \text{ s}^{-1}$ ; recombination rate,  $k_r = 1.90 \times 10^{-13} \text{ ions}^{-1} \text{ m}^3 \text{ s}^{-1}$ ; ionization rate,  $k_i = 1.09 \times 10^{20} \text{ ions m}^{-3} \text{ s}^{-1}$ ; and flame area,  $A_f = 3.90 \times 10^{-3} \text{ m}^2$  (see Ref. [16] for details).

function of frequency and field strength [Fig. 3(b)], where  $I(t)$  is the measured current,  $V(t)$  is the applied voltage, and  $\langle \rangle$  denotes a time average. In the absence of the flame, the dissipation rate is negligible, as expected for an ideal capacitor; the measured dissipation rate thus characterizes the electric response of the flame itself [16].

At low frequencies,  $\Phi$  approaches a constant value corresponding to the oscillation average of the dc current-voltage relationship  $I_{\text{dc}}(V)$  in Fig. 2(b), that is,  $\Phi \approx \langle I_{\text{dc}}(V(t)) \cdot V(t) \rangle$ . Above a critical frequency [dashed curve in Fig. 3(b)], the dissipation rate increases by a factor of  $\sim 5$  at the highest frequencies ( $\sim 1$  kHz); this increase suggests a transition in the structure of the plasma due to the ac field.

## V. DISCUSSION

Electrohydrodynamic flows are driven by an electric force  $f = \rho E$ , which enters into the Navier-Stokes equations

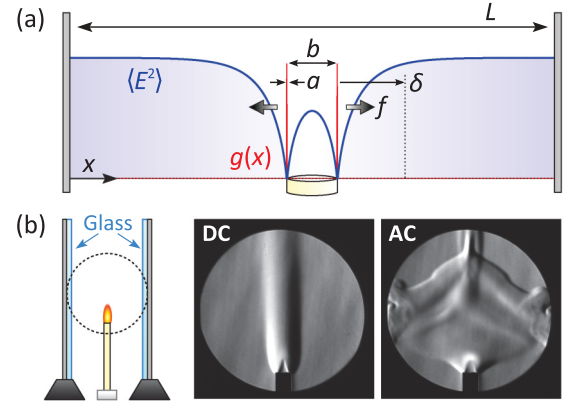


FIG. 4. (Color online) (a) Schematic illustration of the 1D model showing the ionization region  $g(x)$  and the time-averaged field squared  $\langle E^2 \rangle$ . (b) Electrohydrodynamic response of the flame using glass-insulated electrodes for static ( $E_0 = 75$  kV/m; left) and oscillatory ( $E_0 = 75$  kV<sub>rms</sub>/m,  $\nu = 800$  Hz; right) fields.

governing fluid motion. For simplicity, we consider the one-dimensional (1D) geometry illustrated in Fig. 4(a). Gauss's law implies that the electric force can be expressed as  $f(x,t) = \epsilon_0 \partial E^2(x,t) / \partial x$ . Averaging in time over one period of oscillation gives  $\langle f \rangle = \epsilon_0 d \langle E^2 \rangle / dx$ . For the experimental conditions, the field inside the flame is negligible,  $\langle E^2 \rangle \approx 0$ , due to screening by mobile charged species. Far from the flame, the average field strength approaches that of the applied field,  $\langle E^2 \rangle \approx E_0^2$ . The transition of  $\langle E^2 \rangle$  from 0 to  $E_0^2$  occurs across some region of size  $\delta$  within which the electric force is localized (see below). Furthermore, the force is directed outward from the flame in both directions (i.e., from regions of weak field to regions of strong field, in qualitative agreement with the gas jets observed in experiment).

To estimate the gas velocities induced by the steady electric force, we define a characteristic pressure drop  $\Delta p \approx \epsilon_0 E_0^2$  by integrating the force from inside the flame to some point far from the flame. Bernoulli's principle then implies a characteristic velocity of  $u \approx (2\epsilon_0 / \rho_f)^{1/2} E_0$ , which is identical to that derived for static fields.

To determine the length scale  $\delta$  over which the force is distributed, we must consider the details of charge transport in and around the flame. We consider the following model describing the production and consumption of ions within the flame and their transient migration in the field [16]:

$$\frac{\partial n_{\pm}}{\partial t} + \frac{\partial}{\partial x} (\pm K n_{\pm} E) = k_i g(x) - k_r n_+ n_-, \quad (1)$$

$$\frac{\partial E}{\partial x} = \frac{e}{\epsilon_0} (n_+ - n_-), \quad \int_0^L E dx = \sqrt{2} L E_0 \cos(\omega t). \quad (2)$$

Here the charge carriers are assumed to be monovalent ions with equal mobilities  $\pm K \sim 10^{-4} \text{ m}^2 \text{ V}^{-1} \text{ s}^{-1}$ ,<sup>1</sup> the flame is represented by a localized region of ionization  $g(x)$  with a characteristic thickness  $a \sim 10^{-4}$  m [Fig. 4(a)] and magnitude

<sup>1</sup>For ion-doped flames, the symmetry of the gas jets induced by static fields [Fig. 2(b)] suggests that positive and negative ions have similar mobilities. In general, this is not the case (e.g., for premixed flames with large electron densities or for sooting flames).

$k_i \sim 10^{20}$  ions  $\text{m}^{-3} \text{s}^{-1}$  [19]. Ions are consumed through a second-order recombination process with rate constant  $k_r \sim 10^{-13}$  ions $^{-1} \text{m}^3 \text{s}^{-1}$  [19] or by perfectly absorbing electrodes at the system boundaries. Remarkably, this simple model predicts the average dissipation rate as a function of both frequency and field strength, in quantitative agreement with experiments [Fig. 3(b), solid curves].

Further analysis [16] reveals the length scale over which ions are redistributed by the field:  $\delta \sim K E_0 / \kappa \omega$ , where  $\kappa = (\epsilon_0 k_r / e K)^{1/2} \sim 0.3$  is a dimensionless parameter characterizing the relative rates of ion recombination [ $k_r n_0$ , where  $n_0 = (k_i / k_r)^{1/2}$ ] and ion screening ( $e K n_0 / \epsilon_0$ ). Briefly, we rewrite Eq. (1) in terms of the total ion density  $n_s = n_+ + n_-$  and the charge density  $n_d = n_+ - n_-$ , retaining only the dominant terms:

$$\frac{\partial}{\partial x}(K n_d E) \approx -\frac{1}{4} k_r n_s^2, \quad \frac{\partial n_d}{\partial t} + \frac{\partial}{\partial x}(K n_s E) \approx 0. \quad (3)$$

Approximating  $\partial/\partial t$  as  $\omega$ ,  $\partial/\partial x$  as  $\delta^{-1}$ , and field strength by  $E_0$ , Eqs. (2) and (3) yield the characteristic length scale  $\delta \sim K E_0 / \kappa \omega$ , ion density  $n_s \sim \epsilon_0 \omega / e K$ , and charge density  $n_d \sim \kappa \epsilon_0 \omega / e K$ . Examining the magnitude of the neglected terms, this dominant balance governs charge transport outside of the flame [where  $g(x) \sim 0$ ] provided  $\delta \ll L$  and  $\kappa \ll 1$ .

From a microscopic perspective, ions generated within the reaction zone migrate a distance  $\delta$  under the influence of the field before recombining. The migration of a single ion creates an impulse (force multiplied by time) of order  $\delta e / K$ , which is transferred to the neutral gas through molecular collisions. Multiplying this impulse by the net flux of ions leaving the ionization region yields the pressure difference  $\Delta p$  driving the flow. Using the scaling arguments above, the ion flux  $K n_d E$  may be approximated as  $\omega \kappa \epsilon_0 E_0 / e$  such that  $\Delta p \sim \epsilon_0 E_0^2$ , in agreement with the macroscopic derivation above.

When  $\delta$  is larger than  $L$  [ $\omega \ll K E_0 / \kappa L$ ; dashed curve in Fig. 3(b)], ions are consumed at the absorbing electrodes and the dissipation rate is identical to that observed for static fields averaged over one period of oscillation, namely,  $\Phi_{\text{low}} \approx [6\sqrt{2}L^3/\pi(L-b)^3]A_f \epsilon_0 K E_0^3$ , where  $A_f$  is the characteristic area of the flame (needed to convert the results of the 1D model into three dimensions) and  $b$  is the width of the flame

[see Fig. 4(a)]. Above a critical frequency (i.e., when  $\delta \ll L$  or  $\omega \gg K E_0 / \kappa L$ ), ions are instead consumed via chemical recombination processes within a thin region surrounding the flame (e.g.,  $\delta \sim 5$  mm for  $\nu = 1$  kHz and  $E_0 = 100$  kV/m). In this limit, the average dissipation rate increases to  $\Phi_{\text{high}} = (4\sqrt{2}/\kappa)A_f \epsilon_0 K E_0^3$  and no longer depends on the position of the electrodes (i.e., on  $L$ ).

Consequently, and in contrast to flows driven by static fields, ac electric winds do not require electrical contact between the flame and the surrounding electrodes. This independence is illustrated in Fig. 4(b), in which the electrodes have been covered with an electrically insulating material. Upon application of a static field, charge rapidly accumulates on the insulating surfaces, screens the applied field, and prevents the formation of electric winds. The response to an ac field is unchanged.

At even higher frequencies namely, for  $\omega > e K n_0 / \epsilon_0$ , the field varies faster than the time required for ions to redistribute and screen the field within the flame. No flows are expected at such frequencies. For the flame plasmas described here, the ion density is  $n_0 \sim 10^{16}$ – $10^{17}$  ions  $\text{m}^{-3}$  [16], and electric winds are expected only for frequencies  $\nu < 10$ – $100$  kHz.

## VI. CONCLUSION

ac fields induce forces localized at the surface of methane flames to create steady electric winds. Importantly, these results provide a basis for the electrode-free manipulation and control of combustion processes, e.g., by electromagnetic waves. Beyond the symmetric flows detailed here, our preliminary results indicate that directional flows can also be achieved by varying the geometry of the applied field.

## ACKNOWLEDGMENTS

This work was supported by the Defense Advanced Research Projects Agency under Grant No. W944NF-09-1-0005, by the National Science Foundation under Grant No. NSF-DMS0907985, and by the US Department of Energy through the Non-equilibrium Energy Research Center under Grant No. DE-SC0000989.

- 
- [1] J. Lawton and F. Weinberg, *Electrical Aspects of Combustion* (Oxford University Press, Oxford, 1969).
- [2] R. C. Waterfall, R. He, N. B. White, and C. M. Beck, *Meas. Sci. Technol.* **7**, 369 (1996).
- [3] K. G. Payne and F. J. Weinberg, *Proc. R. Soc. London Ser. A* **250**, 316 (1959).
- [4] S. H. Won, M. S. Cha, C. S. Park, and S. H. Chung, *Proc. Combust. Inst.* **31**, 963 (2007).
- [5] H. C. Jagers and A. von Engel, *Combust. Flame* **16**, 275 (1971).
- [6] S. M. Starikovskaia, *J. Phys. D: Appl. Phys.* **39**, R265 (2006).
- [7] M. Robinson, *Am. J. Phys.* **30**, 366 (1962).
- [8] J. Lawton and F. J. Weinberg, *Proc. R. Soc. London Ser. A* **277**, 468 (1964).
- [9] M. Rickard, D. Dunn-Rankin, F. Weinberg, and F. Carleton, *J. Electrostat.* **64**, 368 (2006).
- [10] M. K. Kim, S. K. Ryu, S. H. Won, and S. H. Chung, *Combust. Flame* **157**, 17 (2010).
- [11] M. K. Kim, S. H. Chung, and H. H. Kim, *Proc. Combust. Inst.* **33**, 1137 (2011).
- [12] M. Saito, T. Arai, and M. Arai, *Combust. Flame* **119**, 356 (1999).
- [13] R. M. Clements and P. R. Smy, *J. Appl. Phys.* **40**, 4553 (1969).
- [14] J. W. Daily and C. Chan, *Combust. Flame* **33**, 47 (1978).
- [15] D. R. Jonassen, G. S. Settles, and M. D. Tronosky, *Opt. Lasers Eng.* **44**, 190 (2006).
- [16] See Supplemental Material at <http://link.aps.org/supplemental/10.1103/PhysRevE.86.036314> for details on (a) schlieren image processing, (b) ac dissipation measurements, (c) Langmuir probe measurements, and (d) the charge transport model..
- [17] J. M. Goodings, D. K. Bohme, and C. W. Ng, *Combust. Flame* **36**, 27 (1979).
- [18] J. M. Goodings, D. K. Bohme, and C. W. Ng, *Combust. Flame* **36**, 45 (1979).
- [19] A. B. Fialkov, *Prog. Energy Combust. Sci.* **23**, 399 (1997).